

Cholesteryl ester transfer protein inhibitory oxoacetamido-benzamide derivatives: Glide docking, pharmacophore mapping, and synthesis

Reema Abu Khalaf^{1*}, Areej NasrAllah¹, Wassan Jarrar¹, Dima A. Sabbah¹

¹Department of Pharmacy, Faculty of Pharmacy, Al-Zaytoonah University of Jordan, Amman, Jordan

Dyslipidemia is an abnormal lipid profile associated with many common diseases, including coronary heart disease and atherosclerosis. Cholesteryl ester transfer protein (CETP) is a hydrophobic plasma glycoprotein that is responsible for the transfer of cholesteryl ester from high-density lipoprotein athero-protective particles to pro-atherogenic very low-density lipoprotein and low-density lipoprotein particles. The requirement for new CETP inhibitors, which block this process has driven our current work. Here, the synthesis as well as the ligand-based and structure-based design of seven oxoacetamido-benzamides **9a–g** with CETP inhibitory activity is described. An *in vitro* study demonstrated that most of these compounds have appreciable CETP inhibitory activity. Compound **9g** showed the highest inhibitory activity against CETP with an IC_{50} of 0.96 μ M. Glide docking data for compounds **9a–g** and torcetrapib provide evidence that they are accommodated in the CETP active site where hydrophobic interactions drive ligand/CETP complex formation. Furthermore, compounds **9a–g** match the features of known CETP active inhibitors, providing a rationale for their high docking scores against the CETP binding domain. Therefore, these oxoacetamido-benzamides show potential for use as novel CETP inhibitors.

Keywords: CETP Inhibitors. Cholesteryl ester transfer protein. Dyslipidemia. Glide docking. Oxoacetamido-benzamides. Pharmacophoric features.

INTRODUCTION

Cardiovascular diseases, including coronary heart disease, cerebrovascular disease, peripheral arterial disease, rheumatic and congenital heart diseases, and venous thromboembolism, are a leading cause of death globally (Stewart, Manmathan, Wilkinson, 2017). One important risk factor for cardiovascular diseases is dyslipidemia, defined as high levels of low-density lipoprotein cholesterol (LDL) and triglycerides (TG) and low levels of high-density lipoprotein cholesterol (HDL) (Sarzynski *et al.*, 2015). The underlying causes of dyslipidemias include genetic and lifestyle factors. Familial hypercholesterolemia is a genetic condition

characterized by a mutation in the LDL-receptor, leading to the accumulation of LDL in the blood (Lozano *et al.*, 2016). Hyperlipidemia is a disorder characterized by high levels of LDL and/or very low-density lipoprotein cholesterol (VLDL) (Nelson, 2013). Hypertriglyceridemia is characterized by high levels of TG (> 150 mg/dL) or ≥ 1.7 mmol/L (Perez-Martinez *et al.*, 2016). Many lipid disorders are associated with lifestyle factors, such as lack of exercise, consuming high-saturated fat diet, metabolic disorders, and drug therapy (e.g., immunosuppressants) (Patel, Brocks, 2010; Zhang *et al.*, 2016). However, suitable lifestyle changes, along with drug therapy, can lead to a 30% – 40% reduction in coronary heart disease mortality (Gurr, Harwood, Frayn, 2008; Clark *et al.*, 2012).

Cholesteryl ester transfer protein (CETP) is a plasma glycoprotein with 476 amino acid residues, produced mostly in the liver and secreted into the circulation. The crystal structure of CETP (PDB ID: 4EWS, resolution

*Correspondence: R. Abu Khalaf. Department of Pharmacy. Faculty of Pharmacy. Al-Zaytoonah University of Jordan, Amman, Jordan. Phone: +962-64291511, Ext 280. Fax: 00962-64291432. E-mail: reema.abukhalaf@zuj.edu.jo or rima_abu_khalaf@yahoo.com. ORCID ID: <https://orcid.org/0000-0002-7797-8918>

of 2.59 Å) comprises a 60 Å-long hydrophobic tunnel occupied by two cholesteryl ester (CE) molecules. Two phospholipid molecules also occupy CETP, and while their polar heads are exposed to plasma, their acyl chains are buried in the hydrophobic tunnel. In addition, CETP has two β -barrel domains at the *N* and *C* termini, each with a twisted sheet and a long α -helix, a central β -sheet between the two β -barrels, and a *C*-terminal α -helix (Mezdour *et al.*, 1994). CETP is involved in reverse cholesterol transport and is responsible for increasing VLDL-triglyceride levels, and subsequently LDL levels, through the transfer of CE from HDL particles to VLDL. An increase in the influx of free fatty acids into the liver causes an increase in the level of VLDL-triglyceride secretion and a decrease in HDL-cholesterol levels (Regieli *et al.*, 2008; Suhy *et al.*, 2014; Yassine *et al.*, 2014; Chirasani, Revanasiddappa, Senapati, 2016). Four CETP inhibitors have reached the clinical trial stage, including torcetrapib, dalcetrapib, evacetrapib, and anacetrapib. While the other three CETP inhibitors demonstrated adverse effects, mainly cardiovascular, anacetrapib showed lower side effects and an enhancement of the lipid profile (Mullard, 2017).

Previously, our group designed and synthesized a range of different CETP inhibitors, including benzylidene-amino methanones (Abu Khalaf *et al.*, 2010), benzylamino methanones (Abu Sheikha *et al.*, 2010), *N*-(4-benzyloxyphenyl)-4-methyl-benzenesulfonamides (Abu Khalaf *et al.*, 2012), *N*-(4-benzylamino-phenyl)-toluene-4-sulfonic acid esters (Abu Khalaf *et al.*, 2012), chlorobenzyl benzamides (Abu Khalaf *et al.*, 2017a), fluorinated benzamides (Abu Khalaf *et al.*, 2017b), and substituted benzyl benzamides (Abu Khalaf *et al.*, 2017c). In an attempt to optimize our previously synthesized CETP inhibitors, compound **A** (% inhibition = 50% at 10 μ M, Figure 1) was chosen as a lead (Abu Khalaf *et al.*, 2017c). New oxoacetamido-benzamide analogs **9a–g** were designed and synthesized by varying the aromatic ring *meta* substitution (H, Cl, OCH₃, CH₃) for the F-atom, in addition to varying the aromatic ring *para* substitution with either trifluoromethoxy or trifluoromethyl groups. These substitutions were followed by an *in vitro* biological evaluation of their activity as CETP inhibitors.

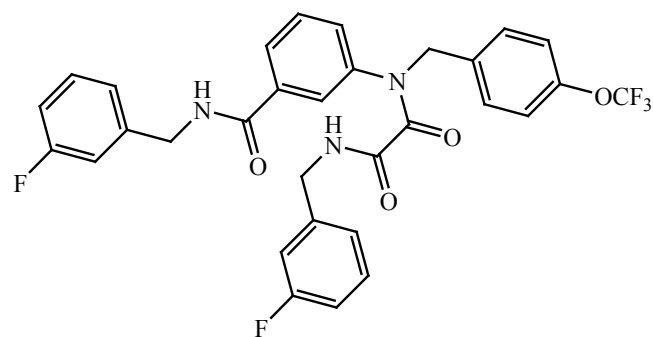


FIGURE 1 - Structure of previously synthesized lead compound **A**.

MATERIAL AND METHODS

Synthesis

All chemicals, reagents, and solvents were of analytical grade. Chemicals and solvents were purchased from the following companies (Alfa Aesar, Acros Organics, Sigma-Aldrich, Fluka, SD fine ChemLimite, Tedia, and Fisher Scientific). Melting points were measured using a Gallenkamp melting point apparatus. Infrared (IR) spectra were recorded using a Shimadzu IR Affinity1 FTIR spectrophotometer. All samples were prepared with potassium bromide and pressed into a disc. ¹H- and ¹³C-Nuclear Magnetic resonance (NMR) spectra were measured using a Bruker, Avance DPX-500 spectrometer, and 400 spectrometer, at The University of Jordan and the Hashemite University, respectively. Chemical shifts are given in δ (ppm) using TMS as an internal reference; the samples were dissolved in deuterated chloroform (CDCl₃) or dimethylsulfoxide (DMSO). An AFLX800TBI Microplate Fluorimeter (BioTek Instruments, Winooski, VT, USA) was used for the *in vitro* bioassay. Thin-layer chromatography (TLC) was performed on 20 \times 20 cm aluminum cards with a layer thickness of 0.2 mm, pre-coated with fluorescent silica gel GF254 DC-alufolien-kieselgel (Fluka Analytical, Germany), and visualized using UV light (at 254 and/or 360 nm).

General procedure for the synthesis of the methyl benzoates intermediates **5a** and **5b**

Preparation of 3-aminobenzoic acid methyl ester (**3**) and the next methyl 3-(4-(trifluoromethoxy)benzylamino) benzoate intermediate (**5a**) were carried out as previously described (Abu Khalaf *et al.*, 2017a; Abu Khalaf *et al.*, 2017b; Abu Khalaf *et al.*, 2017c). Purification was achieved by column chromatography using cyclohexane:ethyl acetate (8.5:1.5) as the eluent. Synthesis of **5b** was commenced by dissolving 2.0 g (13.2 mmol) of ester **3** in 20 mL of dichloromethane (DCM). Then, 1-(bromomethyl)-4-(trifluoromethyl) benzene (**4b**, 6.14 mL, 39.6 mmol), and (TEA 9.3 mL, 66.2 mmol) were added. The mixture was stirred at 20–25°C for 7 days, evaporated, and the intermediate methyl 3-(4-(trifluoromethyl)benzylamino) benzoate (**5b**) was purified by column chromatography using cyclohexane:ethyl acetate (9:1) as the eluent. The intermediate **5b** was obtained as a yellow powder (3.19 g, % yield = 78%); $C_{16}H_{14}F_3NO_2$; mp. 126–127°C; $R_f = 0.4$ (cyclohexane:ethyl acetate, 9:1); 1H -NMR (500 MHz, DMSO- d_6): δ 3.30–3.39 (m, 1H, CH_2NH), 3.79 (s, 3H, OCH_3), 4.42 (d, $J = 6.0$ Hz, 2H, CH_2), 6.74 (t, $J = 7.8$ Hz, 1H, Ar-H), 6.80 (d, $J = 7.8$ Hz, 1H, Ar-H), 7.14–7.21 (m, 2H, Ar-H), 7.57 (d, $J = 8.0$ Hz, 2H, Ar-H), 7.69 (d, $J = 8.1$ Hz, 2H, Ar-H) ppm; ^{13}C -NMR (125 MHz, DMSO- d_6): δ 46.3, 52.4, 113.2, 117.1, 117.2, 123.7, 125.6, 125.9, 128.2, 129.7, 130.8, 145.4, 149.0, 167.1 ppm; IR (KBr): 3394, 3039, 2962, 1712, 1612, 1527, 1334, 1257, 1157 cm^{-1} .

General procedure for the synthesis of the targeted compounds **9a–c**

The preparation of the acyl intermediate **7a** from **5a** was carried out as previously described (Abu Khalaf *et al.*, 2017a; Abu Khalaf *et al.*, 2017b; Abu Khalaf *et al.*, 2017c).

3-(N-(4-(Trifluoromethoxy)benzyl)-2-(benzylamino)-2-oxoacetamido)-N-benzylbenzamide (**9a**)

Benzylamine (**8a**, 0.155 mL, 1.37 mmol), 5 mL of triethylamine, and 10 mL of dichloromethane were added to **7a** (0.64 mmol), then the reaction mixture was stirred

at 20–25°C for 5 days. The crude product was purified by column chromatography using chloroform:ethyl acetate (8.5:1.5) as the eluent.

An off-white viscous liquid was obtained as **9a** (0.180 g, % yield = 43%); $C_{31}H_{26}F_3N_3O_4$; $R_f = 0.29$ (chloroform:ethyl acetate, 8.5:1.5); 1H -NMR (400 MHz, $CDCl_3$): δ 4.31 (d, $J = 4.5$ Hz, 2H, $HNCH_2$), 4.62 (d, $J = 3.9$ Hz, 2H, $HNCH_2$), 4.93 (s, 2H, NCH_2), 6.45 (s, 1H, Ar-H), 7.06 (d, $J = 7.1$ Hz, 1H, Ar-H), 7.12 (d, $J = 7.5$ Hz, 2H, Ar-H), 7.18 (d, $J = 5.0$ Hz, 2H, Ar-H), 7.23 (d, $J = 7.6$ Hz, 2H, Ar-H), 7.29–7.36 (m, 9H, Ar-H), 7.48 (s, 1H, NH), 7.58 (s, 1H, NH), 7.68 (d, $J = 7.1$ Hz, 1H, Ar-H) ppm; ^{13}C -NMR (100 MHz, $CDCl_3$): δ 43.4 (1C, CH_2), 44.3 (1C, CH_2), 54.1 (1C, CH_2), 117.5 (1C, Ar-C), 119.1 (1C, OCF_3), 121.0 (2C, Ar-C), 121.7 (1C, Ar-C), 125.7 (1C, Ar-C), 126.1 (1C, Ar-C), 127.8 (2C, Ar-C), 128.0 (2C, Ar-C), 128.7 (2C, Ar-C), 128.8 (2C, Ar-C), 129.3 (1C, Ar-C), 130.1 (1C, Ar-C), 130.4 (2C, Ar-C), 134.4 (1C, Ar-C), 135.7 (1C, Ar-C), 136.9 (1C, Ar-C), 137.9 (1C, Ar-C), 142.2 (1C, Ar-C), 148.9 (1C, Ar-C), 159.8 (1C, CO), 162.0 (1C, CO), 166.1 (1C, CO) ppm; IR (KBr): 3371, 3248, 3086, 2916, 1643, 1581, 1535, 1481, 1427, 1265, 1226, 1157 cm^{-1} .

N-(3-Methylbenzyl)-3-(2-(3-methylbenzylamino)-N-(4-(trifluoromethoxy)benzyl)-2-oxoacetamido)benzamide (**9b**)

3-Methyl benzylamine (**8c**, 0.15 mL, 1.2 mmol), 5 mL of triethylamine, and 10 mL of dichloromethane were added to **7a** (0.64 mmol), then the reaction mixture was stirred at 20–25°C for 5 days. The crude product was purified by column chromatography using chloroform:acetone (9.5:0.5) as the eluent.

A pale yellow viscous liquid was obtained as **9b** (0.117 g, % yield = 30%); $C_{33}H_{30}F_3N_3O_4$; $R_f = 0.5$ (chloroform:acetone, 9: 1); 1H -NMR (400 MHz, $CDCl_3$): δ 2.34 (s, 3H, CH_3), 2.38 (s, 3H, CH_3), 4.28 (d, $J = 4.3$ Hz, 2H, $HNCH_2$), 4.59 (d, $J = 4.2$ Hz, 2H, $HNCH_2$), 4.94 (s, 2H, NCH_2), 6.37 (s, 1H, Ar-H), 6.94–7.29 (m, 13H, Ar-H), 7.36 (t, $J = 7.5$ Hz, 1H, Ar-H), 7.45 (s, 1H, NH), 7.59 (s, 1H, NH), 7.69 (d, $J = 7.5$ Hz, 1H, Ar-H) ppm; ^{13}C -NMR (100 MHz, $CDCl_3$): δ 21.3 (1C, CH_3), 29.7 (1C, CH_3), 43.5 (1C, $HNCH_2$), 44.3 (1C, $HNCH_2$), 54.2 (1C, NCH_2), 121.0 (2C, Ar-C), 124.9 (1C, OCF_3), 125.1 (1C, Ar-C), 125.7 (1C, Ar-C), 126.1 (1C, Ar-C), 128.5 (1C, Ar-C), 128.5 (2C, Ar-C), 128.5 (1C, Ar-C), 128.6 (1C, Ar-C), 128.7 (1C, Ar-C), 128.8

(1C, Ar-C), 129.3 (1C, Ar-C), 129.8 (1C, Ar-C), 130.0 (1C, Ar-C), 130.4 (1C, Ar-C), 134.4 (1C, Ar-C), 135.8 (1C, Ar-C), 136.8 (1C, Ar-C), 137.7 (1C, Ar-C), 138.5 (1C, Ar-C), 138.6 (1C, Ar-C), 142.3 (1C, Ar-C), 148.9 (1C, Ar-C), 159.6 (1C, CO), 161.9 (1C, CO), 166.1 (1C, CO) ppm; IR (KBr): 3294, 2962, 2924, 1651, 1543, 1265, 1165, 1103 cm^{-1} .

N-(3-Methoxybenzyl)-3-(2-(3-methoxybenzylamino)-*N*-(4-(trifluoromethoxy)benzyl)-2-oxoacetamido)benzamide (**9c**)

3-Methoxy benzylamine (**8d**, 0.15 mL, 1.16 mmol), 5 mL of triethylamine, and 10 mL of dichloromethane were added to **7a** (0.64 mmol); then, the reaction mixture was stirred at 20–25°C for 5 days. The crude product was purified by column chromatography using chloroform:acetone (9.5:0.5) as the eluent.

A pale yellow viscous liquid was obtained as **9c** (0.175 g, % yield = 46%); $\text{C}_{33}\text{H}_{30}\text{F}_3\text{N}_3\text{O}_6$; $R_f = 0.3$ (chloroform:acetone, 93:7); $^1\text{H-NMR}$ (400 MHz , CDCl_3): δ 3.78 (s, 3H, OCH_3), 3.82 (s, 3H, OCH_3), 4.28 (s, 2H, HNCH_2), 4.59 (s, 2H, HNCH_2), 4.93 (s, 2H, NCH_2), 6.47 (s, 1H, Ar-*H*), 6.72 (s, 1H, Ar-*H*), 6.76 (d, $J = 7.0 \text{ Hz}$, 1H, Ar-*H*), 6.81 (d, $J = 7.8 \text{ Hz}$, 1H, Ar-*H*), 6.85–6.95 (m, 4H, Ar-*H*), 7.05 (d, $J = 7.2 \text{ Hz}$, 1H, Ar-*H*), 7.12 (d, $J = 7.4 \text{ Hz}$, 2H, Ar-*H*), 7.16–7.31 (m, 3H, Ar-*H*), 7.34 (t, $J = 6.6 \text{ Hz}$, 1H, Ar-*H*), 7.47 (s, 1H, NH), 7.59 (s, 1H, NH), 7.68 (d, $J = 7.3 \text{ Hz}$, 1H, Ar-*H*) ppm; $^{13}\text{C-NMR}$ (100 MHz , CDCl_3): δ 43.4 (1C, HNCH_2), 44.2 (1C, HNCH_2), 54.1 (1C, NCH_2), 55.3 (2C, OCH_3), 113.1 (1C, Ar-C), 113.2 (1C, Ar-C), 113.5 (1C, Ar-C), 113.7 (1C, Ar-C), 119.1 (1C, OCF_3), 120.0 (2C, Ar-C), 120.2 (1C, Ar-C), 121.0 (1C, Ar-C), 121.7 (1C, Ar-C), 125.7 (1C, Ar-C), 126.1 (1C, Ar-C), 129.3 (1C, Ar-C), 129.8 (2C, Ar-C), 129.9 (1C, Ar-C), 130.1 (1C, Ar-C), 130.4 (2C, Ar-C), 134.4 (1C, Ar-C), 135.8 (1C, Ar-C), 138.5 (1C, Ar-C), 139.4 (1C, Ar-C), 142.2 (1C, Ar-C), 148.9 (1C, Ar-C), 159.9 (1C, CO), 162.0 (1C, CO), 166.2 (1C, CO) ppm; IR (KBr): 3317, 3070, 2931, 1651, 1589, 1442, 1404, 1319, 1265, 1157 cm^{-1} .

General procedure for the synthesis of the targeted compounds 9d–g

Methyl 3-(4-(trifluoromethyl)benzylamino) benzoate (**5b**, 0.25 g) was hydrolyzed to benzoic acid **6b**, as reported previously (Abu Khalaf *et al.*, 2017a; Abu Khalaf *et al.*,

2017b; Abu Khalaf *et al.*, 2017c). Subsequently, **6b** (0.2 g, 0.64 mmol) was dissolved in 10 mL of dichloromethane and then oxalyl chloride (**2**, 0.11 mL, 1.2 mmol, $(\text{COCl})_2$) was added. The reaction was left under stirring for 5 days at 50–60°C. The reaction mixture was then evaporated to obtain the acyl intermediate **7b**.

3-(*N*-(4-(Trifluoromethyl)benzyl)-2-(benzylamino)-2-oxoacetamido)-*N* benzylbenzamide (**9d**)

Next, benzylamine (**8a**, 0.12 mL, 1.14 mmol), 5 mL of triethylamine, and 10 mL of dichloromethane were added to **7b**, and then the reaction mixture was stirred at 20–25°C for 5 days. The crude product was purified by column chromatography using cyclohexane:ethyl acetate (6:4) as the eluent.

A white sticky powder was obtained as **9d** (0.1 g, % yield = 31%); $\text{C}_{31}\text{H}_{26}\text{F}_3\text{N}_3\text{O}_3$; mp. 79–80°C; $R_f = 0.29$ (chloroform:ethyl acetate, 8.5:1.5); $^1\text{H-NMR}$ (500 MHz , DMSO-d_6): δ 4.09 (d, $J = 5.3 \text{ Hz}$, 2H, HNCH_2), 4.43 (d, $J = 5.0 \text{ Hz}$, 2H, HNCH_2), 5.04 (s, 2H, NCH_2), 6.83 (d, $J = 6.5 \text{ Hz}$, 1H, Ar-*H*), 6.95 (d, $J = 7.95 \text{ Hz}$, 1H, Ar-*H*), 7.12 (d, $J = 6.9 \text{ Hz}$, 3H, Ar-*H*), 7.20 (m, 2H, Ar-*H*), 7.25 (t, $J = 5.65 \text{ Hz}$, 4H, Ar-*H*), 7.43 (t, 3H, Ar-*H*), 7.60 (m, 2H, Ar-*H*), 7.78 (d, $J = 7.6 \text{ Hz}$, 1H, Ar-*H*), 7.83 (s, 1H, Ar-*H*), 9.00 (t, $J = 5.85 \text{ Hz}$, 1H, NH), 9.18 (t, $J = 10.9 \text{ Hz}$, 1H, NH) ppm; $^{13}\text{C-NMR}$ (125 MHz , DMSO-d_6): δ 41.9 (1C, HNCH_2), 43.1 (1C, HNCH_2), 51.4 (1C, NCH_2), 123.7 (1C, CF_3), 125.5 (1C, Ar-C), 126.9 (1C, Ar-C), 127.0 (1C, Ar-C), 127.1 (1C, Ar-C), 127.2 (1C, Ar-C), 127.4 (2C, Ar-C), 127.5 (2C, Ar-C), 128.3 (1C, Ar-C), 128.4 (2C, Ar-C), 128.5 (1C, Ar-C), 128.8 (1C, Ar-C), 128.9 (1C, Ar-C), 135.8 (1C, Ar-C), 138.5 (1C, Ar-C), 139.4 (1C, Ar-C), 139.8 (1C, Ar-C), 139.9 (1C, Ar-C), 141.0 (1C, Ar-C), 141.8 (1C, Ar-C), 163.4 (1C, Ar-C), 164.1 (1C, Ar-C), 165.4 (1C, CO), 165.5 (1C, CO), 167.4 (1C, CO) ppm; IR (KBr): 3332, 3263, 2962, 1651, 1543, 1411, 1327 cm^{-1} .

N-(3-Chlorobenzyl)-3-(2-(3-chlorobenzylamino)-*N*-(4(trifluoromethyl)benzyl)-2-oxoacetamido)benzamide (**9e**)

Next, 3-chlorobenzylamine (**8b**, 0.25 mL, 2.05 mmol), 5 mL of triethylamine, and 10 mL of dichloromethane were added to **7b**, then the reaction

mixture was stirred at 20–25°C for 5 days. The crude product was purified by column chromatography using chloroform:ethyl acetate (7.5:2.5) as the eluent.

A white sticky powder was obtained as **9e** (0.1 g, % yield = 22%); C₃₁H₂₄Cl₂F₃N₃O₃; mp. 89–90°C; R_f = 0.46 (chloroform:ethyl acetate, 7.5:2.5); ¹H-NMR (400 MHz_Z, CDCl₃): δ 4.30 (d, *J* = 4.9 Hz, 2H, HNCH₂), 4.60 (d, *J* = 4.6 Hz, 2H, HNCH₂), 5.00 (s, 2H, NCH₂), 6.50 (s, 1H, Ar-H), 7.08 (d, *J* = 8.4 Hz, 2H, Ar-H), 7.17 (s, 1H, Ar-H), 7.20–7.45 (m, 9H, Ar-H, NH), 7.55 (d, *J* = 7.6 Hz, 3H, Ar-H), 7.64 (s, 1H, NH), 7.68 (d, *J* = 7.3 Hz, 1H, Ar-H) ppm; ¹³C-NMR (100 MHz_Z, CDCl₃): δ 42.8 (1C, CH₂), 43.6 (1C, CH₂), 54.4 (1C, CH₂), 122.6 (1C, CF₃), 125.3 (1C, Ar-C), 125.6 (2C, Ar-C), 125.6 (1C, Ar-C), 125.7 (1C, Ar-C), 125.8 (1C, Ar-C), 126.0 (1C, Ar-C), 126.1 (1C, Ar-C), 127.8 (1C, Ar-C), 127.9 (1C, Ar-C), 128.0 (2C, Ar-C), 129.1 (2C, Ar-C), 129.5 (1C, Ar-C), 130.1 (2C, Ar-C), 134.5 (1C, Ar-C), 134.6 (1C, Ar-C), 135.5 (1C, Ar-C), 138.9 (1C, Ar-C), 139.5 (1C, Ar-C), 140.0 (1C, Ar-C), 142.2 (1C, Ar-C), 159.8 (1C, CO), 162.0 (1C, CO), 166.1 (1C, CO) ppm; IR (KBr): 3394, 3263, 3070, 2962, 1651, 1581, 1535, 1481, 1435, 1327 cm⁻¹.

N-(3-Methylbenzyl)-3-(2-(3-methylbenzylamino)-*N*-(4-(trifluoromethyl)benzyl)-2-oxoacetamido)benzamide (**9f**)

Next, 3-methylbenzylamine (**8c**, 0.14 mL, 1.14 mmol), 5 mL of triethylamine, and 10 mL of dichloromethane were added to **7b**, then the reaction mixture was stirred at 20–25°C for 5 days. The crude product was purified by column chromatography using chloroform: acetone (9:1) as the eluent.

An off-white viscous liquid was obtained as **9f** (0.08 g, % yield = 22%); C₃₃H₃₀F₃N₃O₃; R_f = 0.4 (cyclohexane:ethyl acetate, 9:1); ¹H-NMR (400 MHz_Z, CDCl₃): δ 2.34 (s, 3H, CH₃), 2.38 (s, 3H, CH₃), 4.29 (d, *J* = 6.0 Hz, 2H, HNCH₂), 4.59 (d, *J* = 5.7 Hz, 2H, HNCH₂), 5.00 (s, 2H, NCH₂), 6.33 (s, 1H, Ar-H), 6.9–7.04 (m, 2H, Ar-H), 7.05–7.20 (m, 5H, Ar-H), 7.21–7.28 (m, 2H, Ar-H), 7.34–7.43 (m, 4H, Ar-H, NH), 7.55 (d, *J* = 8.0 Hz, 2H, Ar-H), 7.63 (s, 1H, NH), 7.68 (d, *J* = 7.6 Hz, 1H, Ar-H) ppm; ¹³C-NMR (100 MHz_Z, CDCl₃): δ 21.4 (1C, CH₃), 29.7 (1C, CH₃), 43.5 (1C, HNCH₂), 44.3 (1C, HNCH₂), 54.5 (1C, NCH₂), 124.9 (1C, CF₃), 125.1 (2C, Ar-C), 125.6

(2C, Ar-C), 126.0 (1C, Ar-C), 128.5 (2C, Ar-C), 128.6 (1C, Ar-C), 128.7 (2C, Ar-C), 128.8 (1C, Ar-C), 129.0 (1C, Ar-C), 129.1 (2C, Ar-C), 129.3 (1C, Ar-C), 130.0 (1C, Ar-C), 135.8 (1C, Ar-C), 136.8 (1C, Ar-C), 137.7 (1C, Ar-C), 138.5 (1C, Ar-C), 138.6 (1C, Ar-C), 139.7 (1C, Ar-C), 142.4 (1C, Ar-C), 148.0 (1C, Ar-C), 159.5 (1C, CO), 162.3 (1C, CO), 166.1 (1C, CO) ppm; IR (KBr): 3302, 3062, 2924, 1658, 1543, 1404, 1327 cm⁻¹.

N-(3-Methoxybenzyl)-3-(2-(3-methoxybenzylamino)-*N*-(4-(trifluoromethyl)benzyl)-2-oxoacetamido)benzamide (**9g**)

Next, 3-methoxybenzylamine (**8d**, 0.1 mL, 0.77 mmol), 5 mL of triethylamine, and 10 mL of dichloromethane were added to **7b**, then the reaction mixture was stirred at 20–25°C for 5 days. The crude product was purified by column chromatography using chloroform:acetone (97:3) as the eluent.

An off-white sticky powder was obtained as **9g** (0.05 g, % yield = 17%); C₃₃H₃₀F₃N₃O₅; mp. 109–111°C; R_f = 0.4 (cyclohexane:ethyl acetate, 9:1); ¹H-NMR (400 MHz_Z, DMSO-d₆): δ 3.70 (s, 3H, OCH₃), 3.72 (s, 3H, OCH₃), 4.10 (d, *J* = 5.5 Hz, 2H, HNCH₂), 4.46 (d, *J* = 5.8 Hz, 2H, HNCH₂), 5.09 (s, 2H, NCH₂), 6.42 (d, *J* = 7.2 Hz, 1H, Ar-H), 6.67 (s, 1H, Ar-H), 6.74 (d, *J* = 9.7 Hz, 1H, Ar-H), 6.81 (d, *J* = 2.3 Hz, 1H, Ar-H), 6.84–6.90 (m, 1H, Ar-H), 7.08 (t, *J* = 7.8 Hz, 1H, Ar-H), 7.22 (t, *J* = 8.0 Hz, 1H, Ar-H), 7.32–7.36 (m, 2H, Ar-H), 7.48 (d, *J* = 8.1 Hz, 1H, Ar-H), 7.67–7.74 (m, 4H, Ar-H), 7.80 (d, *J* = 2.1 Hz, 1H, Ar-H), 7.87 (s, 1H, Ar-H), 9.03 (t, *J* = 5.6 Hz, 1H, NH), 9.24 (t, *J* = 5.5 Hz, 1H, NH) ppm; ¹³C-NMR (100 MHz_Z, DMSO-d₆): δ 42.0 (1C, HNCH₂), 43.1 (1C, HNCH₂), 51.3 (1C, NCH₂), 55.4 (2C, OCH₃), 112.6 (1C, Ar-C), 112.7 (1C, Ar-C), 113.4 (1C, Ar-C), 113.5 (1C, Ar-C), 119.6 (1C, Ar-C), 119.9 (1C, Ar-C), 125.8 (1C, CF₃), 126.4 (1C, Ar-C), 126.8 (1C, Ar-C), 129.0 (2C, Ar-C), 129.1 (2C, Ar-C), 129.5 (1C, Ar-C), 129.8 (1C, Ar-C), 130.4 (1C, Ar-C), 132.1 (2C, Ar-C), 132.2 (1C, Ar-C), 135.8 (1C, Ar-C), 140.1 (1C, Ar-C), 140.9 (1C, Ar-C), 141.5 (1C, Ar-C), 159.6 (1C, Ar-C), 159.8 (1C, Ar-C), 163.3 (1C, CO), 165.6 (1C, CO), 167.5 (1C, CO) ppm; IR (KBr): 3302, 3070, 2962, 2916, 1651, 1589, 1543, 1411, 1327 cm⁻¹; HR-MS (ESI, negative mode) *m/z* [M-1]⁺ 604.21043 (C₃₃H₂₉F₃N₃O₅ requires 604.21376).

Computational methods

Preparation of protein structures

The coordinates of CETP (PDB ID: 4EWS, resolution of 2.59 Å) (Liu *et al.*, 2012) were obtained from the RCSB Protein Data Bank. The CETP structure was prepared and energetically minimized using the protein preparation wizard (Protein Preparation Wizard, 2016) in the Schrödinger software to optimize H-bond interactions.

Preparation of ligand structures

The synthesized compounds (ligands) were modeled based on the structure of the co-crystallized ligand (ORP) in 4EWS (Liu *et al.*, 2012). Ligands were built using the MAESTRO build panel and energetically minimized in MacroModel script (Protein Preparation Wizard, 2016) using the OPLS2005 force field.

Glide docking

The grid file for CETP was extracted using the Glide Grid Generation protocol (Protein Preparation Wizard, 2016) with the embedded ligand as the centroid. The van der Waals scaling factor for the nonpolar atoms was calibrated to 0.8 to promote flexibility for the protein side chains. No water molecules were considered. All other parameters were scaled to default. The binding energies were used to determine the docking scores (kcal/mol). A highly negative docking score indicates a better binding interaction.

In vitro CETP inhibition bioassay

An aliquot of rabbit serum (1 µL) was mixed with the testing sample (2 µL). Next, donor molecule (5 µL) and acceptor molecule (5 µL) in the assay buffer were added, mixed well, and the volume was adjusted to 200 µL using the assay buffer.

The mixture was incubated at 37°C for 1 h. The fluorescence intensity (excitation λ: 480 nm; emission λ: 511 nm) was measured using a FLX800TBI Microplate Fluorimeter (BioTek Instruments, Winooski, VT, USA).

The synthesized molecules were first dissolved in DMSO to yield 10 mM stock solutions. The solutions were then diluted to the required concentration using DMSO. The concentration of all synthesized compounds was adjusted to 10 µM; CETP activity was not affected by DMSO at the final concentration used in diluted solutions. The percentage of residual CETP activity was identified in the presence and absence of the tested molecules. Torcetrapib was used as a positive inhibitor to estimate CETP inhibition (0.08 µM concentration). Negative control samples without rabbit serum were used for the contrast background. The experimental protocol and all measurements were carried out in duplicate.

The percentage inhibition of CETP by the synthesized compounds was calculated using the following equation (Abu Khalaf *et al.*, 2017a):

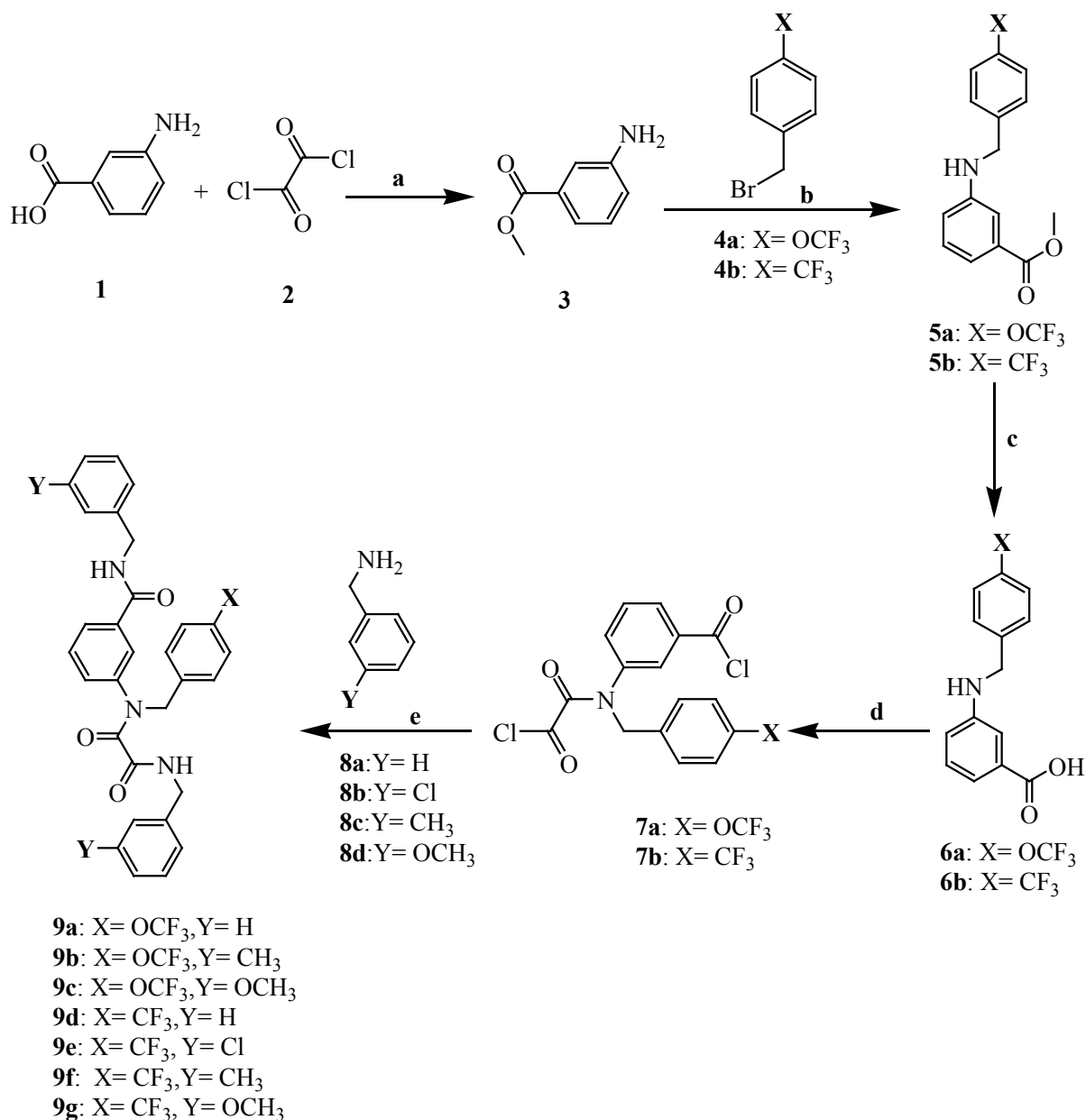
$$\% \text{ Inhibition} = [1 - \frac{[(\text{Inhibitor reading} - \text{Blank reading}) / (\text{Positive control} - \text{Negative control})]}{1}] * 100$$

The mid-range experimental dose groups responded in a linear fashion with respect to dose, and IC₅₀ values were determined from this linear portion of the curve. The equation of this dose-response line was correctly determined by plotting the percentage inhibition of CETP against the log concentration of the tested compound, allowing the IC₅₀ values to be calculated accurately. Primary screening of the inhibitory activity of the synthesized compounds at 10 µM concentration was performed; 10 µM was chosen according to our previous studies on CETP inhibitors. Because several inhibitors demonstrated a % inhibition of approximately 90%, these compounds were also assayed at three additional lower concentrations (5.0 µM, 1.0 µM, and 0.5 µM), to obtain CETP % inhibition values above and below the IC₅₀ value. A line of best-fit was then drawn. The correlation coefficient (R²) of the corresponding dose-response line was calculated (see Table I).

RESULTS AND DISCUSSION

Synthesis

A series of oxoacetamido-benzamides **9a–g** were synthesized as shown in **Scheme 1**.



SCHEME 1 - Synthesis of the targeted oxoacetamido-benzamides **9a-g**. Reagents and conditions: (a) CH₃OH/reflux (60–70°C), 24 h, (b) DCM, TEA, RT, 5 days, (c) (1) 1M NaOH (100°C), overnight, (2) Concentrated HCl, (d) (COCl)₂ /reflux (60–70°C), DCM, 4 days, (e) TEA, DCM, RT, 5 days.

The synthesis was commenced with the activation of the carboxylic acid moiety of 3-aminobenzoic acid (**1**) using oxalyl chloride (**2**) in the presence of methanol to produce acyl chloride. Subsequently, nucleophilic attack of the OH group of methanol on the carbonyl carbon of the acyl chloride produced the methyl ester protecting group **3**.

Next, the amine nitrogen of 3-amino benzoic acid methyl ester (**3**) attacked the partially positive methylene

group of benzyl bromide **4a** or **4b** in the presence of DCM as a solvent to produce the substituted 3-benzylamino benzoic acid methyl ester intermediates **5a** or **5b**. Triethylamine was used as an acid scavenger (HBr). It was found that **5a** (46% yield) was produced in a lower yield than **5b** (78% yield).

Deprotection of the carboxylic acid groups of 3-aminobenzoic acid methyl ester intermediates **5a**

and **5b** was carried out by alkaline hydrolysis using 1M NaOH under reflux, followed by neutralization with concentrated HCl.

Then, reactivation of the carboxylic acid moiety of 3-benzylamino benzoic acid intermediates **6a** or **6b** was performed using oxalyl chloride (**2**) to produce the acyl chloride derivatives in the presence of DCM and the tetrahedral structure left as HCl, CO₂, and CO gases. Additionally, the lone pair of electrons of the nitrogen atom of intermediates **6a** and **6b** attacked the partially positive carbonyl carbon moiety of oxalyl chloride (**2**), where the chloride ion was left as a good leaving group.

Subsequently, amide formation was attained by the nucleophilic attack of the amine moiety of one of the used benzylamines **8a–d** on the partially positive carbonyl

carbon of the previously produced acyl chlorides to obtain the targeted benzamide derivatives **9a–g**.

In vitro CETP inhibition bioassay

The results of the *in vitro* CETP inhibition assay, presented in Table I, demonstrate that most of the targeted compounds have an appreciable activity against CETP at a concentration of 10 μM. Three of them (**9c**, **9e**, and **9g**) were found to have a % inhibition of approximately 90% at 10 μM concentration. Therefore, the inhibitory activities of **9c**, **9e**, and **9g** were evaluated at lower concentrations (5.0 μM, 1.0 μM, and 0.5 μM), and their IC₅₀ values were determined (Table I).

TABLE I - *In vitro* bioactivities of the synthesized oxoacetamido-benzamides **9a–g**

Synthesized compound	% Inhibition (at 10.0 μM)	% Inhibition (at 5.0 μM)	% Inhibition (at 1.0 μM)	% Inhibition (at 0.5 μM)	IC ₅₀ (μM)
9a	71.7± 0.4	ND	ND	ND	ND
9b	84.4± 0.7	ND	ND	ND	ND
9c	92.7± 0.6	69.8±0.7	35.3± 0.2	18.4±0.4	1.89 (R ² = 0.99)**
9d	62.7± 0.5	ND	ND	ND	ND
9e	92.3± 0.8	68.3±0.5	26.7± 0.5	16.2±0.4	2.16 (R ² = 0.99)**
9f	20.0± 0.5	ND	ND	ND	ND
9g	90.4± 0.7	75.2±0.6	55.9± 0.4	33.7±0.6	0.96 (R ² = 0.99)**
Torcetrapib (ORP)	88.2*± 0.8	ND	ND	ND	0.04

ND: not determined. *: at concentration of 0.08 μM.

** : This value represents the correlation coefficient of the corresponding dose-response line at four concentrations.

As can be seen in Table I, most of the synthesized compounds demonstrated comparable bioactivities (within the same range). As a general observation, benzamides with *p*-OCF₃ groups (**9a–c**) demonstrated slightly higher CETP inhibition at 10 μM concentration than those with the *p*-CF₃ moiety (**9d–g**), especially when they were substituted with the *m*-CH₃ group (**9b** and **9f**). Furthermore, in comparison to the previously synthesized *p*-substituted analogs (Abu Khalaf *et al.*, 2017c), the *m*-CH₃ group in **9b** demonstrated a higher % inhibition (84.4%) than its *p*-CH₃ substituted analog (62.1%), and compound **9c** with the *m*-OCH₃ moiety

demonstrated higher % inhibition (92.7%) than its *p*-OCH₃ substituted analog (65.8%).

Docking study

To identify the structural basis for CETP inhibition by the co-crystallized ligand (ORP: torcetrapib) and the targeted compounds **9a–g**, the glide docking approach was used (Friesner *et al.*, 2004; Friesner *et al.*, 2006) against CETP (PDB ID: 4EWS) (Liu *et al.*, 2012). The Glide docking data for compounds **9a–g** and ORP

demonstrated that each of these compounds could be accommodated in the active site of 4EWS. Furthermore, as shown in Figure 2, the docked **9a** model can be superimposed on the coordinates of ORP (torcetrapib).

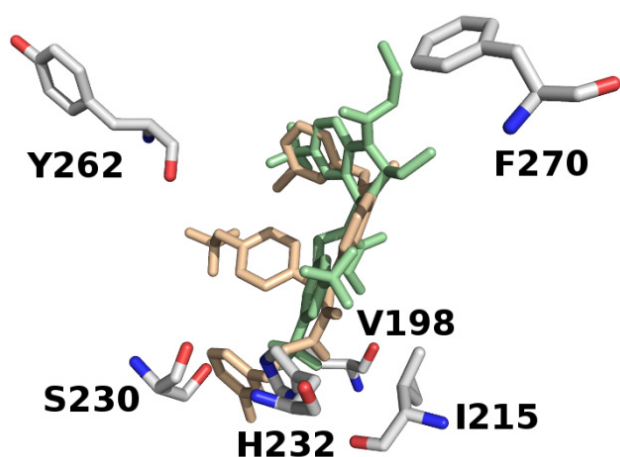


FIGURE 2 - Superimposition of the Glide docked **9a** model (represented in gold color) and the co-crystallized ligand ORP (green color). H atoms and some of key binding residues are hidden for clarity. Picture captured using PYMOL.

The Glide docking data suggested that hydrophobic interactions drive ligand/4EWS complex formation (Table II; Figure 3 and 4; Supplementary Figures 1S and 2S). Additionally, the backbones of **9e** and **9f** formed an H-bond with S230 (Figures 3S).

TABLE II - The Glide docking scores (kcal/mol) of **9a–g** and ORP

Compound	Glide docking scores (kcal/mol)	H-Bond
9a	-10.62	NA
9b	-11.80	NA
9c	-11.37	NA
9d	-11.63	NA
9e	-11.41	S230
9f	-12.06	S230
9g	-12.58	NA
Torcetrapib (ORP)	-10.57	NA

NA: not available.

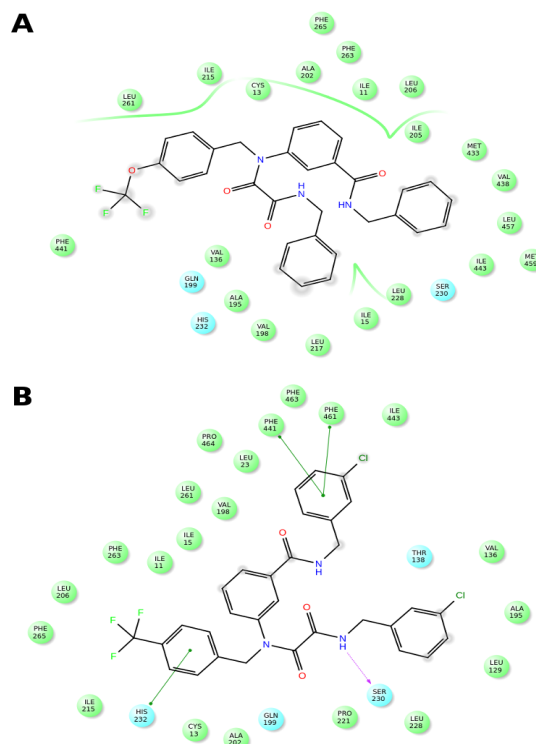


FIGURE 3 - The ligand/4EWS complex of (A) **9a** and (B) **9e**. Hydrophobic residues are colored green. Picture visualized using MAESTRO (Protein Preparation Wizard, 2016).

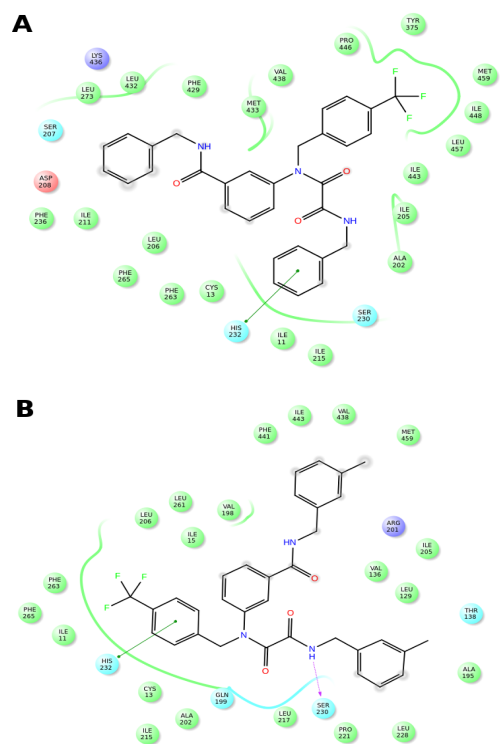


FIGURE 4 - The ligand/4EWS complex of (A) **9d** and (B) **9f**. The hydrophobic lining is colored green. Picture visualized by MAESTRO (Protein Preparation Wizard, 2016).

The high binding scores obtained for compounds **9a–g** against 4EWS indicate that this scaffold has potential inhibitory activity against CETP. Furthermore, the small difference (2 kcal/mol) observed between the binding affinity of the co-crystallized ligand (ORP: torcetrapib) and the binding affinities of **9a–g** provides further evidence of the significance of this scaffold for CETP inhibition.

To assess the performance of the Glide program, the structure of the docked ORP model was compared with the experimental ORP coordinates from the 4EWS crystal structure (Liu *et al.*, 2012). Figure 5 demonstrates the superimposition of the Glide-produced ORP model with the experimental structure from 4EWS. The RMSD for the heavy atoms of ORP in these structures was 1.534 Å. These results indicate that Glide docking is capable of generating the experimental conformation from the 4EWS crystal structure, and thus evaluating the location of ligand binding.

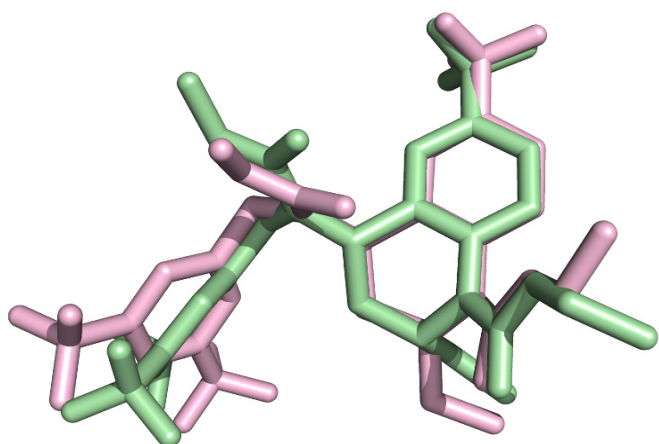


FIGURE 5 - The superimposition of the Glide-docked ORP model with the experimental structure in 4EWS. The native structure is green colored and the docked model is pink colored. Picture visualized by PYMOL.

The *in vitro* biological data demonstrated that compound **9c** tailored with X= *p*-OCF₃ and Y= *m*-OCH₃ moieties exhibited promising CETP inhibition. According to the modeling results, the H-bond acceptor and/or hydrophobic pocket interacted with the *m*-OCH₃ and *p*-OCF₃ motifs in **9c**. Moreover, the high inhibitory activity of compound **9e** substituted with X= *p*-CF₃ and Y= *m*-Cl groups demonstrated the significance of hydrophobic interactions on 4EWS/ligand complex formation and CETP inhibition. Additionally, compound

9g substituted with X= *p*-CF₃ and Y= *m*-OCH₃ showed comparable inhibitory activity to that of **9e**. This finding provided further evidence for the dominance of hydrophobic interactions in the 4EWS binding domain. A comparison of the activities of compounds **9a–c** indicated that the *m*-H-bond acceptor moiety is essential for the activity of analogs bearing *p*-OCF₃.

In contrast, the absence of *m*-Cl, as exemplified in compound **9d**, weakened the inhibitory activity, and the replacement of *m*-Cl with *m*-CH₃ as in compound **9f** decreased the activity further. Together, the observed inhibitory activities of compounds **9d–g** provide evidence that the *m*-electron-withdrawing moiety might induce CETP inhibitory activity. Nevertheless, *m*-Cl and *m*-CH₃ are hydrophobic and isosteres of each other; the *m*-electron-withdrawing effect was significant for the inhibitory activity of derivatives tailored to *p*-CF₃.

Pharmacophore mapping

To investigate the core structures of compounds **9a–g** and their motifs, these structures were scanned against the CETP active inhibitor pharmacophore model (Abu Khalaf *et al.*, 2017a). Compounds **9a–g** matched the features of CETP active inhibitors (Figure 6), providing a rationale for their high docking scores against the CETP binding domain. Additionally, the accommodation of compounds **9a–g** in the CETP binding domain explained their inhibitory activity.

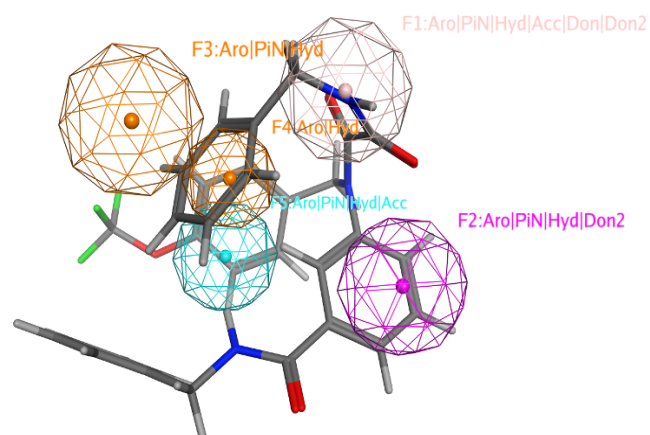


FIGURE 6 - The pharmacophore model of CETP active inhibitor with **9a**. Aro, aromatic rings; Acc, H-bond acceptor; Don, H-bond donor; Cat, cationic group; PiN, π -ring; and Hyd, hydrophobic groups. Picture captured by MOE (The Molecular Operating Environment, 2016).

CONCLUSIONS

The present study identified oxoacetamido-benzamide as a new scaffold targeting CETP activity. The targeted benzamides were found to express similar bioactivities, with compound **9g** showing an IC_{50} of 0.96 μ M. The results of the study suggest that the presence of a *p*-trifluoromethoxy group may enhance CETP inhibitory activity. Future optimization of the structure of these inhibitors is required to enhance their physicochemical properties and to clarify the structure-activity relationship.

ACKNOWLEDGMENTS

The authors acknowledge the Deanship of Scientific Research at Al-Zaytoonah University of Jordan for sponsoring this project.

CONFLICT OF INTEREST

The authors declare no conflicts of interest.

REFERENCES

- Abu Khalaf R, Abd El-Aziz H, Sabbah D, Albadawi G, Abu Sheikha G. CETP inhibitory activity of chlorobenzyl benzamides: QPLD docking, pharmacophore mapping, and synthesis. *Lett Drug Des Discov*. 2017a;14(12):1391-400.
- Abu Khalaf R, Abu Sheikha G, Al-Sha'er M, Albadawi G, Taha M. Design, synthesis, and biological evaluation of sulfonic acid ester and benzenesulfonamide derivatives as potential CETP inhibitors. *Med Chem Res*. 2012;21(11):3669-80.
- Abu Khalaf R, Abu Sheikha G, Bustanji Y, Taha MO. Discovery of new cholesteryl ester transfer protein inhibitors via ligand-based pharmacophore modeling and QSAR analysis followed by synthetic exploration. *Eur J Med Chem*. 2010;45(4):1598-617.
- Abu Khalaf R, Al-Rawashdeh S, Sabbah D, Abu Sheikha G. Molecular docking and pharmacophore modeling studies of fluorinated benzamides as potential CETP Inhibitors. *Med Chem*. 2017b;13(3):239-53.
- Abu Khalaf R, Sabbah D, Al-Shalabi E, Bishtawi S, Albadawi G, Abu Sheikha G. Synthesis, biological evaluation, and molecular modeling study of substituted benzyl benzamides as CETP inhibitors. *Arch Pharm*. 2017c;350(12):e1700204.
- Abu Sheikha G, Abu Khalaf R, Melhem A, Albadawi G. Design, synthesis, and biological evaluation of benzylamino-methanone based cholesteryl ester transfer protein inhibitors. *Molecules*. 2010;15(8):5721-33.
- Chirasani VR, Revanasiddappa PD, Senapati S. Structural Plasticity of Cholesteryl Ester Transfer Protein Assists the Lipid Transfer Activity. *J Biol Chem*. 2016;291(37):19462-73.
- Clark MA, Finkel R, Rey JA, Whalen K. Lippincott's illustrated reviews. *Pharmacology*, 5th ed.; MD: Wolters Kluwer Health/Lippincott Williams & Wilkins: Baltimore, 2012.
- Friesner RA, Banks JL, Murphy RB, Halgren TA, Klicic JJ, Mainz DT, et al. Glide: A new approach for rapid, accurate docking and scoring. 1. Method and assessment of docking accuracy. *J Med Chem*. 2004;47(7):1739-49.
- Friesner RA, Murphy RB, Repasky MP, Frye LL, Greenwood JR, Halgren Ta, et al. Extra precision glide: Docking and scoring incorporating a model of hydrophobic enclosure for protein-ligand complexes. *J Med Chem*. 2006;49(21):6177-96.
- Gurr MI, Harwood JL, Frayn KN. *Lipid Biochemistry: An Introduction*, 5th ed.; Wiley-Blackwell, 2008.
- Liu S, Mistry A, Reynolds JM, Lloyd DB, Grifför MC, Perry DA, et al. Crystal structures of cholesteryl ester transfer protein in complex with inhibitors. *J Biol Chem*. 2012;287(44):37321-9.
- Lozano P, Henrikson NB, Dunn J, Morrison CC, Nguyen M, Blasi PR et al. Lipid Screening in Childhood and Adolescence for Detection of Familial Hypercholesterolemia: A Systematic Evidence Review for the U.S. Preventive Services Task Force. *Evidence Synthesis*. 2016, No. 141, Report No.: 14-05204-EF-2, Rockville (MD): Agency for Healthcare Research and Quality (US).
- Mezdour H, Kora I, Parra HJ, Tartar A, Marcel YL, Fruchart JC. Two-site enzyme immunoassay of cholesteryl ester transfer protein with monoclonal and oligoclonal antibodies. *Clin Chem*. 1994;40(4):593-7.
- Mullard A. CETP inhibitors stumble on. *Nat Rev Drug Discov*. 2017;16(10):669.
- Nelson RH. Hyperlipidemia as a risk factor for cardiovascular disease. *Prim Care*. 2013;40(1):195-211.
- Patel JP, Brocks DR. Effect of experimental hyperlipidaemia on the electrocardiographic effects of repeated doses of halofantrine in rats. *Br J Pharmacol*. 2010;161(6):1427-40.
- Perez-Martinez P, Alcalá-Díaz JF, Kabagambe EK, Garcia-Rios A, Tsai MY, Delgado-Lista J et al. Assessment of postprandial triglycerides in clinical practice: Validation in a general population and coronary heart disease patients. *J Clin Lipidol*. 2016;10(5):1163-71.

Protein Preparation Wizard, Maestro, Macromodel, QPLD-dock, and Pymol. Schrödinger, LLC, Portland, OR, U.S.A., 2016.

Regieli JJ, Jukema JW, Grobbee DE, Kastelein JJP, Kuivenhoven JA, Zwinderman AH, et al. CETP genotype predicts increased mortality in statin-treated men with proven cardiovascular disease: an adverse pharmacogenetic interaction. *Eur Heart J.* 2008;29(22):2792-9.

Sarzynski MA, Schuna JM, Carnethon MR, Jacobs DR, Lewis CE, Quesenberry CP, et al. Association of fitness with incident dyslipidemias over 25 years in the coronary artery risk development in young adults study. *Am J Prev Med.* 2015;49(5):745-52.

Stewart J, Manmathan G, Wilkinson P. Primary prevention of cardiovascular disease: A review of contemporary guidance and literature. *JRSM Cardiovasc Dis.* 2017;6:1-9.

Suhy A, Hartmann K, Newman L, Papp A, Toneff T, Hook V, et al. Genetic variants affecting alternative splicing of human cholesteryl ester transfer protein. *Biochem Biophys Res Commun.* 2014;443(4):1270-4.

The Molecular Operating Environment, Chemical Computing Group, Inc Montreal, Quebec, Canada, 2016.

Yassine HN, Belopolskaya A, Schall C, Stump CS, Lau SS, Reaven PD. Enhanced cholesterol efflux to HDL through the ABCA1 transporter in hypertriglyceridemia of type 2 diabetes. *Metabolism.* 2014;63(5):727-34.

Zhang X, Zhang Y, Liu Y, Wang J, Xu Q, Yu X, et al. Medium-chain triglycerides promote macrophage reverse cholesterol transport and improve atherosclerosis in ApoE-deficient mice fed a high-fat diet. *Nutr Res.* 2016;36(9):964-73.

Received for publication on 18th February 2020

Accepted for publication on 26th October 2020

SUPPLEMENTARY MATERIAL

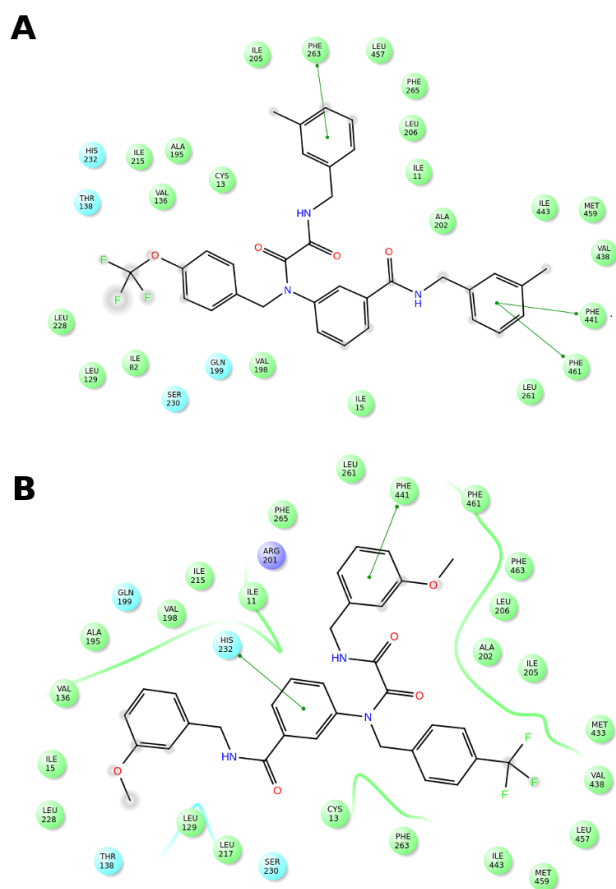


FIGURE 15 - The ligand/4EWS complex of (A) 9b and (B) 9g. The hydrophobic lining is green colored. Picture made by MAESTRO (Protein Preparation Wizard, 2016)

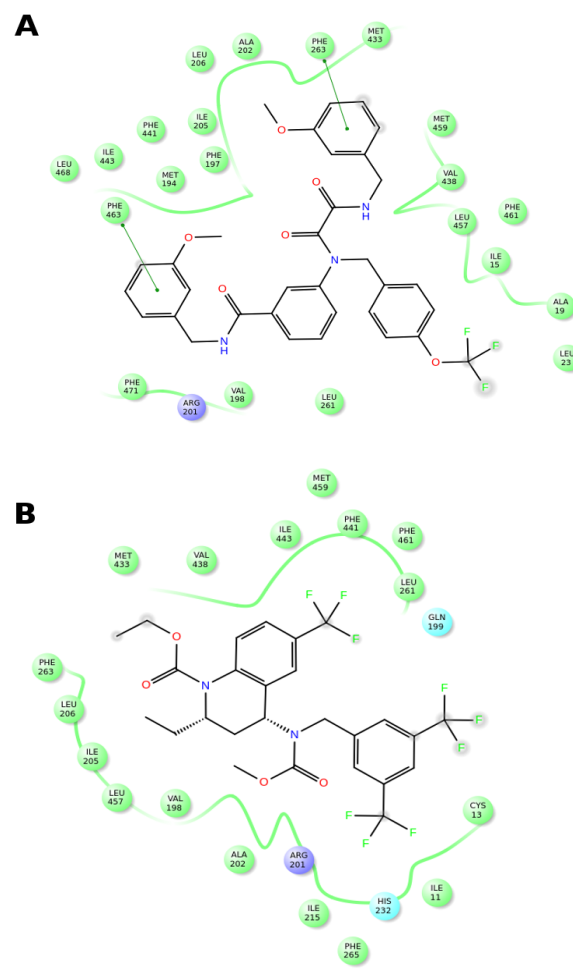


FIGURE 25 - The ligand/4EWS complex of (A) 9c and (B) 9d. The hydrophobic lining is green colored. Picture made by MAESTRO (Protein Preparation Wizard, 2016)

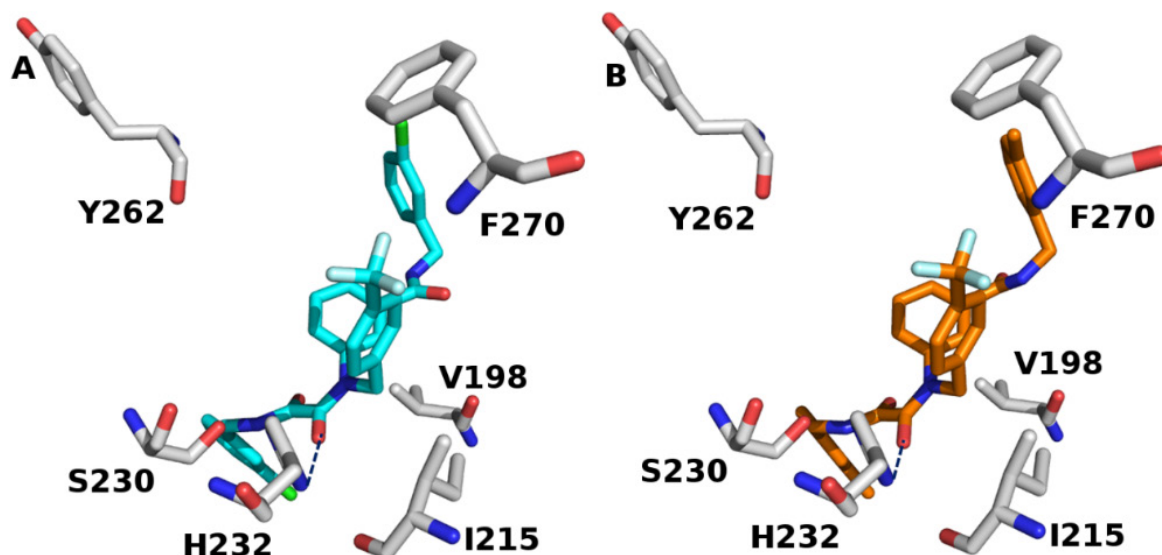


FIGURE 3S - Glide docked poses of (A) 9e (B) 9f in 4EWS binding site. H-Bond is represented in blue dotted line. Some key binding residues are disclosed and H atoms are invisible for clarification. Picture captured by PYMOL

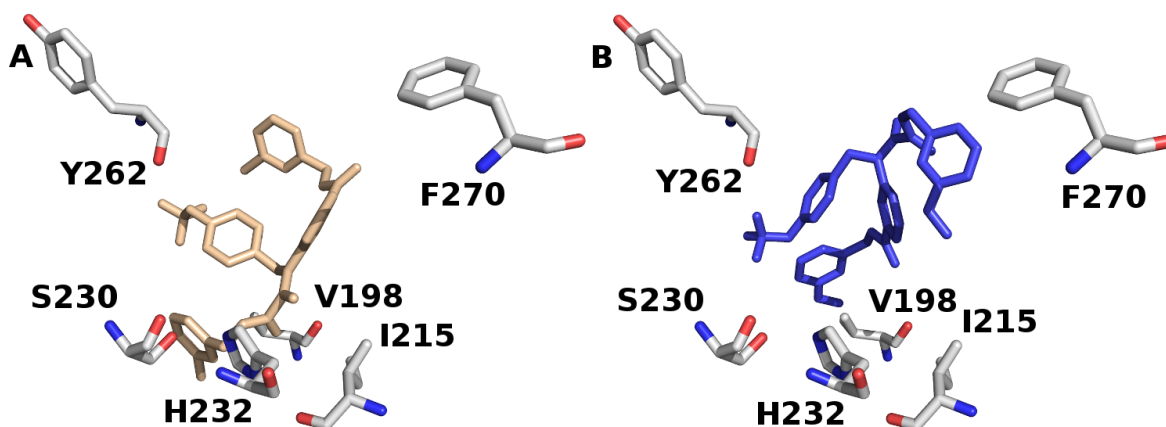


FIGURE 4S - Glide docked poses of (A) 9c (B) 9d in 4EWS binding site. Some key binding residues are disclosed and H atoms are invisible for clarification. Picture captured by PYMOL

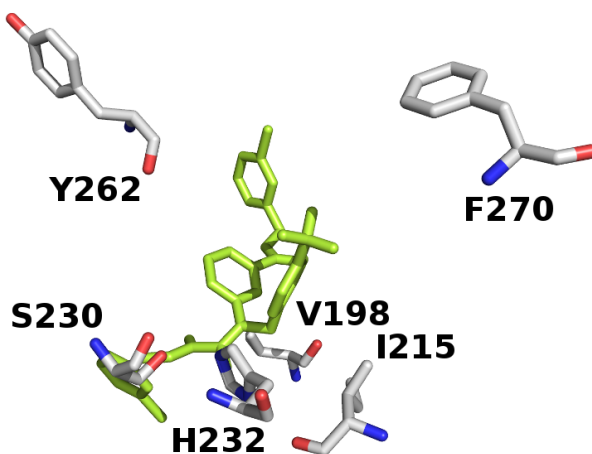


FIGURE 5S - Glide docked poses of 9g in 4EWS binding site. Some key binding residues are disclosed and H atoms are invisible for clarification. Picture captured by PYMOL